inorganics

MDPI

Article

Local Energy Minima and Density of Energy Barriers in Dense Clusters of Magnetic Nanoparticles

Natalia L. Gorn, Elena K. Semenova and Dmitry Berkov *

General Numerics Research Lab, Kahlaische Str. 4, D-07745 Jena, Germany
* Correspondence: d.berkov@general-numerics-rl.de

Abstract: In this paper, we focus on the properties of local energy minima and energy barriers in immobilized dense clusters of magnetic nanoparticles. Understanding of these features is highly interesting both for the fundamental physics of disordered systems with long-range interparticle interaction and for numerous applications of modern ferrofluids consisting of such clusters. In particular, it is needed to predict the ac-susceptibility of these systems and their magnetization relaxation after a sudden change in the external field, because both processes occur via magnetization jumps over energy barriers that separate the energy minima. Due to the exponential increase in the corresponding jump time with barrier height ($t_{sw} \sim \exp(\Delta E/kT)$), direct Langevin dynamics simulations of this process are not feasible. For this reason, we have developed efficient numerical methods both for finding as many energy minima as possible and for the reliable evaluation of energy barriers between them. Our results for the distribution of overlaps between the local energy minima imply that there is no spin-glass state in such clusters even when they consist of particles with a small anisotropy. Further, we show that the distributions of energy barrier heights are qualitatively different for clusters of particles with small, intermediate, and large anisotropies, which has important consequences for the magnetization dynamics of these systems.

Keywords: magnetic nanoparticles; energy minima; energy barriers; spin glass; magnetization dynamics; particle clusters; particle aggregates; ferrofluids; numerical simulations

Citation: Gorn, N.L.; Semenova, E.K.; Berkov, D. Local Energy Minima and Density of Energy Barriers in Dense Clusters of Magnetic Nanoparticles. *Inorganics* **2024**, *12*, 329. https://doi.org/10.3390/inorganics12120329

Academic Editor: Peter Burger

Received: 19 November 2024
Revised: 10 December 2024
Accepted: 13 December 2024
Published: 17 December 2024

1. Introduction

Functionalized nanoparticles have become indispensable in modern technology, especially in medical diagnostics and therapy (see, for example, the reviews [1–5] and the literature cited therein). Ferromagnetic nanoparticles with sizes ranging from about 10 nm to approximately 200 nm, which under normal conditions remain in a (roughly) single-domain state, play a particularly important role [6–9]. Due to their high magnetic moment, these particles can be controlled by an external magnetic field, which otherwise has relatively little influence on processes in living organisms, since these organisms (except for some exotic bacteria) do not contain ferromagnetic materials.

For this reason, systems of magnetic nanoparticles in a carrier fluid (ferrofluids) are already actively used for many purposes, or relevant methods are being intensively researched. These topics include (i) targeted drug delivery using a gradient magnetic field [4,7,9], (ii) magnetic hyperthermia [1,2,10,11] isolation and enrichment for diagnostic and therapeutic purposes [8], (iii) imaging techniques for the location of magnetic nanoparticles in tissue (Magnetic Particle Imaging) for diagnostic purposes [12,13], etc.

This variety of applications requires extensive theoretical analysis to understand the processes in many-particle magnetic systems and to provide recommendations to manufacturers and users of these substances. This analysis is complicated by several factors, mainly by long-range magnetodipolar interparticle interaction, but also by the relatively wide distribution of particle parameters (size, shape, magnetization, and magnetic anisotropy) and the different types of particle coatings required for various applications.

Significant efforts have been undertaken in this direction over the past two decades. The behavior of many-particle systems composed of individual particles is relatively well understood from the theoretical point of view. In the early simple models, magnetic particles were treated as magnetic dipoles with a fixed moment. This approximation assumes that the magnetic anisotropy of a single particle is so strong that the magnetic moment is always aligned along the particle's anisotropy axis. This model is still widely used, for example, to study the dynamic susceptibility of concentrated ferrofluids, to understand the effects of magnetodipolar interaction on the dynamics of individual particles, and to understand the formation of particle aggregates [14–16].

However, the assumption regarding the high anisotropy is incorrect in most cases and is particularly inaccurate for the magnetite particles most commonly used in applications. Qualitatively better models were developed in [17–19], where the internal degrees of freedom in such particles—in the first line the rotation of the magnetic moment relative to the particle itself—are taken into account, and significant progress in the modeling of these systems was achieved. In particular, magnetic relaxation due to mechanical particle rotation (Brownian relaxation) and jumps of the magnetic moment over the anisotropy barrier (Néel relaxation) were studied (see the review [19]), and energy absorption in particles with moderate anisotropy was calculated [20,21].

However, in the most common case, magnetic many-particle systems are composed not of individual separate nanoparticles but of multicore clusters containing from several tens to several hundreds of nanoparticles (nanocores) embedded in a common polymer shell. In a typical ferrofluid, the formation of these aggregates takes place already during its manufacturing due to the magnetodipolar attraction of individual particles and is very difficult to prevent. These dense systems fundamentally differ from those made of individual nanoparticles because the magnetodipolar interaction within such clusters is very strong.

Ferrofluids consisting of many-particle clusters are potentially very attractive for several applications because such clusters can have a much higher magnetic moment than a single nanoparticle. Moreover, this moment can be induced in much smaller external fields than those that are required to saturate the magnetization of single particles with the same size as a many-particle cluster. Consequently, attempts have been made to use such clusters in hyperthermia [22,23], for drug delivery in magnetic gradient fields, and in the cell separation [4].

For this reason, substantial effort has been undertaken in recent years to achieve a better understanding of quasistatic and dynamic remagnetization processes in densely packed magnetic clusters. The task is really challenging, because the long-range magnetodipolar interaction within such a cluster should be correctly taken into account. Concerning quasistatic properties, dependence of the cluster magnetic moment on the applied field [24], the force acting on a multicore particle in a magnetic field [25], and hysteresis loops of systems composed of various clusters have been studied (see, e.g., [11,26,27]). Among dynamics processes, energy absorption in nanoparticle aggregates [23,28,29], magnetic relaxation within microscopic times [30], and relaxation in dense nanoparticle systems on various time scales have been measured and simulated (see [16,31–35] and references therein). The latter papers are briefly discussed below by analyzing the nature of the spin-glass-like properties of these systems.

However, physical understanding of dense ensembles of nanoparticles is still insufficient. The reasons for this deficit are two-fold. On the one hand, considerable experimental effort is required to prepare concentrated nanoparticle systems with a narrow size distribution of particles, which is a necessary prerequisite for the reliable interpretation of the measured properties. On the other hand, simulations of the magnetization dynamics on various time scales are usually performed via Monte Carlo methods, which have well-known difficulties in escaping local energy minima at low temperatures.

For these reasons, in this paper we have performed detailed studies of the local energy minima and the energy barrier landscape in densely packed clusters of magnetic

nanoparticles. We have employed simulation methods which provide the corresponding information for $T = 0$, so that our results can be considered as the limiting case of low-temperature system properties.

This paper is organized as follows. In Section 2, we explain our methods of finding local energy minima and analyze the distribution of their overlaps; relation of the obtained results to the expected spin-glass features of these systems is discussed afterwards. Section 3 presents our version of the nudged elastic band method used to compute optimal trajectories between local minima. In the same section, we introduce the terms of 'true' and 'false' optimal transitions and explain how we distinguish between these two transition kinds. In Section 4, we present the distribution of energy barriers for clusters composed of particles with very different single-particle anisotropies and discuss corresponding results in connection with magnetic relaxation in such systems. Our findings are summarized in the Conclusions (Section 6).

2. Search for Local Energy Minima of Multicore Nanoclusters

Before studying the transition between the local energy minima in clusters of nanoparticles, we need an efficient algorithm to create dense clusters of randomly packed particles (in our case spheres). For this purpose, we started with the geometrical algorithm described in [36]. We strongly optimized the original method by introducing a list of nearest neighbours, so that the operation count of the algorithm became $\sim N_\mathrm{p}$, where N_p is the desired number of particles in the cluster. Furthermore, the method was extended to allow the generation of clusters with any form (in this research, we consider spherical clusters). Using this improved method, we could generate clusters that have the packing density ≈ 0.5 and contain a nearly arbitrary number of particles; in our simulations, we used clusters with a particle number up to 2000. We also note that, according to [30], different algorithms for the cluster formation lead to clusters with magnetic properties that are nearly the same, so that the choice of a particular method does not affect the physical results.

Here, we assume that multicore nanoclusters are immobilized, so that particle coordinates do not depend on time. To determine the energy minima in this situation, we calculate the total energy of the system E_tot, which is composed of the energy in the external field E_ext, anisotropy energy E_an, and the energy of the magnetodipolar interaction E_dip:

$$\begin{aligned} E_\mathrm{tot} &= E_\mathrm{ext} + E_\mathrm{an} + E_\mathrm{dip} = \\ &- \sum_i \boldsymbol{\mu}_i \mathbf{H}_i^\mathrm{ext} - \sum_i K_i V_i (\mathbf{m_i} \cdot \mathbf{n_i})^2 - \frac{1}{2} \sum_{i \neq j} \boldsymbol{\mu}_i \mathbf{H}_i^\mathrm{dip} \end{aligned} \tag{1}$$

Here, $\boldsymbol{\mu}_i$ denotes the magnetic moment of the i-th particle, $\mathbf{H}_i^\mathrm{ext}$ the external field at this particle, K_i the anisotropy constant, V_i the particle volume, $\mathbf{m}_i = \boldsymbol{\mu}_i / M V_i$ the unit vector of the magnetic moment, and $\mathbf{n}_i$ the unit vectors of the anisotropy axis direction. The form of E_an in (1) corresponds to the uniaxial particle anisotropy type.

Using the constant K and the magnetization of the particle material M, we can define the reduced anisotropy constant $\beta = 2K/M^2$. The value of β allows us to estimate the relation between the magnetodipolar interaction field from the nearest neighbour and the anisotropy field.

The magnetodipolar interaction field $\mathbf{H}_i^\mathrm{dip}$ in the third term denotes the magnetic field at the location of the i-th particle generated by all other particles in the system:

$$\mathbf{H}_i^\mathrm{dip} = \sum_{j \neq i} \frac{3\left(\boldsymbol{\mu}_j \cdot \mathrm{e}_{ij}\right)\mathrm{e}_{ij} - \boldsymbol{\mu}_j}{r_{ij}^3} \tag{2}$$

where $\mathbf{r}_{ij} = \mathbf{r}_i - \mathbf{r}_j$ and $\mathbf{e}_{ij} = \mathbf{r}_{ij}/r_{ij}$.

For our purposes, it is convenient introduce the reduced field $\mathbf{h} = \mathbf{H}/\mathbf{M}$ and to define the reduced energy in units of the maximal anisotropy energy per particle:

$$\tilde{E}_{\text{tot}} = E/KV = \\ -\frac{2}{\beta}\sum_i \mathbf{m}_i\mathbf{h}_i^{\text{ext}} - \sum_i(\mathbf{m_i}\cdot\mathbf{n_i})^2 - \frac{1}{\beta}\sum_{i\neq j}\mathbf{m}_i\mathbf{h}_i^{\text{dip}} \quad (3)$$

The reduced magnetodipolar field $\mathbf{h}_i^{\text{dip}}$ in this context is

$$\mathbf{h}_i^{\text{dip}} = \frac{4\pi}{3}\sum_{j\neq i}\frac{3(\mathbf{m}_j\cdot\mathrm{e}_{ij})\mathrm{e}_{ij} - \mathbf{m}_j}{\tilde{r}_{ij}^3} \quad (4)$$

where the reduced distance is defined in units of the particle radius R: $\tilde{r}_{ij} = r_{ij}/R$.

The total energy E_{tot} (1) should be minimized in order to find metastable states of the system. Although the number of particles in a multicore cluster is usually moderate ($N_{\text{p}} \sim$ 100–1000), we will show below that such a cluster may possess a macroscopically large number of energy minima. For this reason, the choice of the minimization method becomes an important issue.

Standard numerical methods for minimizing functions of many variables (in our case, the system's energy) include the method of steepest descent, the conjugate gradient (CG) method, and various quasi-Newton methods. The method of steepest descent is known for its slow convergence, as it requires many small iterative steps when descending through a long and narrow valley, even for relatively simple energy functions. Quasi-Newton methods require $\sim N^3$ operations per iteration (N being the number of independent variables) for inverting the system's Hessian matrix, which also makes them too slow for the number of variables given above.

For these reasons, the CG method seems to be the most promising candidate among the standard methods. However, in our specific case there is a fundamental problem that significantly complicates their usage. Namely, for the implementation of the CG method for our task, we have to convert the coordinates of magnetic moments from Cartesian coordinates to spherical ones, although the formulas for the effective field and the energy contributions in spherical coordinates are much more complicated. The reason for this conversion is that the magnitude of each magnetic moment must remain constant during the magnetization process ($\mu = MV$). Therefore, its Cartesian coordinates are not independent variables due to the requirement $\mu_x^2 + \mu_y^2 + \mu_z^2 = \text{Const}$. However, construction of a set of conjugate directions in the CG method fails when dependent variables are used.

This transition to spherical coordinates is in principle possible, but it leads to another technical problem: when a particle's moment is close to the polar axis, its small movements can lead to arbitrary changes in the corresponding azimuthal angle. This instability leads to a very slow convergence of the method and often even to a failure in constructing the set of conjugate directions. Bypassing this problem by introducing individual coordinate systems for each particle (which could be performed in our case) leads to excessive technical effort while simultaneously reducing efficiency. Therefore, we decided to apply two other methods that are known from related applications and have to be adapted to the multicore particle system.

These methods are described in detail in our paper [37], but here we briefly repeat the main ideas to make this paper self-contained.

2.1. Method A: Solution of the Equation of Motion

Due to its physical transparency, guaranteed convergence, and the multitude of mathematical methods available for solving systems of ordinary differential equations, this method is very popular in simulating magnetic many-particle systems. The basic idea is

to develop a minimization procedure based on the equations of motion for a magnetic moment in an effective field, usually in the Landau–Lifshitz–Gilbert form:

$$\frac{d\mathbf{m}_i}{d\tau} = -\left(\mathbf{m}_i \times \mathbf{h}_i^{\text{eff}}\right) - \lambda\left(\mathbf{m}_i \times \left(\mathbf{m}_i \times \mathbf{h}_i^{\text{eff}}\right)\right) \tag{5}$$

where the reduced time is $\tau = \gamma M t$, the reduced field is $\mathbf{h} = \mathbf{H}/M$, γ denotes the gyromagnetic ratio, and λ is the damping constant. According to the definition (3), the effective field $\mathbf{h}_i^{\text{eff}}$ is the sum of three contributions: external, anisotropy, and magnetodipolar fields.

Since we are not interested in the magnetization dynamics, but only in the relaxation to equilibrium, we can omit the first (precession) term and solve the system of ordinary differential equations (ODEs), which contains only the energy dissipation term:

$$\frac{d\mathbf{m}_i}{d\tau} = -\lambda \mathbf{m}_i \times (\mathbf{m}_i \times \mathbf{h}_{\text{eff},i}), \tag{6}$$

The evolution of the magnetization governed by this equation should lead us to the local minimum (the nearest one to the starting state), according to the principle of energy dissipation.

There exist a large number of methods for solving such systems of ODEs. For our system, we implemented two Runge–Kutta methods of different orders (RK23 and RK45) and adaptive step size control. The corresponding algorithm was significantly faster than the CG method.

2.2. Method B: Alignment Method

The idea behind this method originates from the basic assumption that particle magnetic moments can only be rotated (i.e., their magnitude cannot be changed). This means that to reach a (meta)stable equilibrium state, each magnetic moment should be aligned parallel to the effective field. In such a state, the torque $T \sim \mathbf{m}_i \times \mathbf{h}_{\text{eff}_i}$ acting on each magnetic moment is zero, and therefore no further rotations of all moments occur. This observation leads to the following method:

(1) For the current state, the effective field on each moment $\mathbf{h}_i^{\text{eff}}$ is calculated;
(2) Each moment is aligned along $\mathbf{h}_i^{\text{eff}}$;
(3) The new effective field is calculated;
(4) We check whether the convergence criterion $\left|\mathbf{m}_i \times \mathbf{h}_i^{\text{eff}}\right| < \epsilon$ is met ($\epsilon \sim 10^{-4}$ is a small threshold). If not, the new magnetization state is accepted, and we return to step (1). If yes, the minimization is successfully completed.

Unfortunately, in its simple form this algorithm can enter into a non-convergent cycle. However, we have observed that in all practical cases, these cycles are very close to a simple oscillatory behavior, which allowed us to implement a more stable version of steps (1)–(3)—see [37] for details.

In our simulations, we employ both methods—the solution of the equation of motion and the alignment method. Our computer experiments show that for systems with a low particle anisotropy, the solution of the equation of motion is more efficient, while for systems with a strong anisotropy the alignment method is faster.

2.3. Number of Energy Minima as a Function of the Particle Number

Before computing the energy barriers between various local minima in a cluster of magnetic nanoparticles, we have to collect a representative set of magnetization states corresponding to these local minima.

For this purpose, we conducted a series of simulations for multicore particle systems, varying the number of nanoparticles in a cluster and the reduced particle anisotropy constant.

For high single-particle anisotropy values $\beta = 2K/M^2 \gg 1$, we expect an exponential growth of the number of found minima with the number of nanoparticles (cores) in a cluster. Indeed, for particles with a high anisotropy the magnetodipolar interaction does not play

any noticeable role (according to the definition of β). Hence, each particle retains its two equivalent energy minima—for moment orientations along the two opposite directions of the anisotropy axis. This means, in turn, that the number of minima for a cluster of N_p particles is $N_\mathrm{min} = 2^{N_\mathrm{p}}$. This dependence was confirmed by our simulations, where we started from arbitrary orientations of magnetic moments and minimized the system energy using the alignment method described in Section 2.2. Corresponding dependence was observed for anisotropies $\beta \geq 10$.

For medium and low anisotropies, a non-exponential dependence $N_\mathrm{min}(N_\mathrm{p})$ could be expected because of the long-range character of the magnetodipolar interaction. Due to this feature, in corresponding many-particle magnetic clusters (where magnetodipolar interparticle interaction is strong compared to the single-particle anisotropy) the number of local minima could increase with the particle number slower than exponentially due to the 'collective' nature of these minima.

In contrast to this expectation, we have also found that for medium and low anisotropy values, the exponential dependency $N_\mathrm{min} \sim \exp(\alpha N_\mathrm{p})$ remains valid, as shown in Figure 1 (note the logarithmic scale of the y axis). It can be seen that for a cluster of particles with the anisotropy $K = 4 \times 10^4\,\mathrm{erg/cm^3}$ and magnetization $M = 800\,\mathrm{G}$—so that the reduced anisotropy is only $\beta = 1.25$—the number of minima exceeds 10^3 already for $N_\mathrm{p} = 35$ nanoparticles. The corresponding coefficient in the exponent α is significantly smaller than $\alpha = \log 2$ for particles with a high anisotropy, but the dependence is clearly exponential.

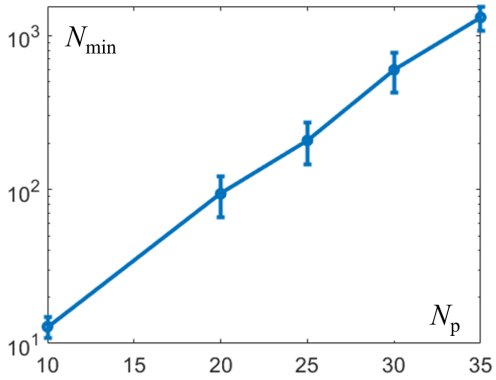

Figure 1. Number of minima for a multicore cluster of particles with the cubic anisotropy $K = 4 \times 10^4$ erg/cm^3, $M = 800$ G (reduced anisotropy $\beta = 1.25$) and the particle radius $R_p = 5$ nm as a function of the number of particles in the cluster (note the logarithmic scale of the y-axis).

Furthermore, assuming that this dependence is due to the formation of sub-clusters consisting of several nanoparticles, each of which acts as a nearly independent quasiparticle with two energy minima, we can estimate the number of particles n_sub in each sub-cluster. Applying the relation $2^{n_\mathrm{sub}} = N_\mathrm{min}$, we obtain from the value $N_\mathrm{min} \approx 10^3$ for $N_\mathrm{p} = 35$ that for this particle number we have $n_\mathrm{sub} \approx 10$ sub-clusters, so that one sub-cluster consists (on average) of $N_\mathrm{p}/n_\mathrm{sub} \approx 3.5$ nanoparticles.

With reference to the next sections, we point out that the exponential growth of the number of minima necessitated a complete change of the standard simulation concept for the search of energy barriers between pairs of energy minima. Indeed, the number of transitions between the minima grows as $N_\mathrm{trans} \sim N_\mathrm{min}^2$, and the effort for computing all barriers for an exponentially large number of energy minima would be unrealistic. Therefore, we abandoned the attempt to capture the complete landscape of minima and developed a method that allowed us to gain statistically relevant information about the entire system through optimal structuring of the energy landscape (see Section 3).

2.4. Absence of the Spin-Glass State in Densely Packed Magnetic Clusters

One of the most interesting questions concerning systems of interacting magnetic nanoparticles is the question of the existence of the spin-glass phase [38,39] in such systems. From the theoretical point of view, the spin-glass state in magnetodipolar ensembles can exist, because such systems possess two necessary (but not sufficient!) prerequisites for the presence of this state—spatial disorder and so-called 'frustration'. The latter term means that a configuration of magnetic moments where the energy of each pair of them is at its minimum does *not* exist. Taking into account that the magnetodipolar interaction energy of two particles depends not only on the interparticle distance, but also on the mutual orientation of their magnetic moments with respect to each other and to the interparticle distance vector (see Equation (2)), frustration is obviously present in these systems. In addition, the magnetodipolar interaction is a long-range one, which also leads to a high complexity of the system's energy landscape.

Strong indications for the existence of the spin-glass phase in systems of magnetic nanoparticles were found in several experimental studies—see, e.g., [31,32,35,40–42]. In these papers, it was shown that disordered systems of fine magnetic particles (and especially corresponding systems with a high volume concentration of particles) demonstrate the dynamic behavior typical for conventional atomic-level spin glasses—in the first place, the so-called 'memory effect' for some specific cooling protocols and 'aging' in magnetic relaxation measurements.

The question concerning the existence of the spin-glass phase in 'magnetodipolar' systems was also studied theoretically by means of Monte Carlo simulations—see the recent very detailed paper of Alonso et al. [43] and references therein. In Ref. [43], the typical 'quasistatic' features of the spin-glass state, namely (i) the characteristic temperature dependence of the magnetization correlation length and (ii) a non-trivial distribution of overlaps between different energy minima were found for some specific particle concentrations at low temperature.

The latter feature—a non-trivial distribution of overlaps—is very important from the theoretical point of view, because a classical definition of a spin glass includes the existence of many local energy minima with very different energies and the hierarchical structure of the manifold of these minima (see the above cited reviews for details). For these reasons, the distribution density of overlaps between different minima in these system should be highly non-trivial (as well as the distribution density of the minima energies).

To check whether densely packed clusters of magnetic nanoparticles possess these features, we performed a further in-depth investigation. Namely, we studied the above-mentioned distribution density of overlaps between two minima in our system. The corresponding overlap is defined as

$$q_{ij} = \frac{1}{N_\mathrm{p}} \sum_{k}^{N_\mathrm{p}} \mathbf{m}_k^{(i)} \mathbf{m}_k^{(j)}, \tag{7}$$

where $\mathbf{m}_k^{(i)}$ is the unit magnetic moment vector of the k-th particle in the i-th energy minimum of the cluster.

The overlap defined this way has a clear physical sense. Namely, for an Ising ferromagnet with two possible orientations of each moment ($m_z = \pm 1$) and two equivalent global energy minima at $T < T_\mathrm{c}$, its possible values are $q_{12} = \pm 1$, so that the distribution density of overlaps in the thermodynamic limit $N_\mathrm{p} \to \infty$ is $P_\mathrm{fm}(q) \sim \delta(q-1) + \delta(q+1)$. For a non-interacting system of magnetic particles with uniaxial anisotropy and randomly oriented anisotropy axes, this density (in the same limit) is $P_\mathrm{mp}(q) \sim \delta(q)$. However, for a 'true' spin glass with a *hierarchical* structure of energy minima, $P(q)$ is highly non-trivial, being a continuous non-zero function between the minimal and maximal possible overlaps q_min and q_max (which are not necessarily ± 1, but not equal to zero) [38,39].

In order to understand the behavior of the distribution density of overlaps $P(q)$ in the thermodynamical limit $N_\mathrm{p} \to \infty$ in our system, we have computed this density for clusters

with increasing particle number, from $N_p = 100$ to $N_p = 2000$. We have studied the case of a small reduced single-particle anisotropy $\beta = 0.5$, because large anisotropies would obviously destroy the spin-glass behavior (each particle will possess two energy minima, independently on the moment orientations of other particles). For all clusters, we have produced $N_{min} = 1000$ different energy minima, starting each time from a new randomly generated initial state. Hence, for building the densities of overlaps $P(q)$ defined in (7), we had to our disposal random realizations of overlap sets containing $N_{ovl} = N_{min}^2 = 10^6$ overlaps each, resulting in a highly accurate estimation of this density.

As an example, the histogram $P(q)$ for the particle number $N_p = 100$ is shown in Figure 2a, together with the corresponding Gaussian fit. It can be seen that $P(q)$ has a perfectly Gaussian shape with very small deviation near $q = 0$ due to the confinement of possible overlap values in the interval $-1 \leq q \leq 1$. This deviation disappears when we increase the number of particles, whereby the histograms become narrower.

The non-trivial structure of the overlap distribution density $P(q)$ assumes that this distribution has at least a non-zero width in the limit $N_p \to \infty$. To find out whether this is the case, we have plotted the dependence of the variance (second moment) σ^2 of $P(q)$ defined as

$$\sigma^2 = \int q^2 P(q) dq \tag{8}$$

on the inverse number of particles $1/N_p$, as shown in Figure 2b. The dashed blue line shown in Figure 2 is the quadratic fit to all data, used to demonstrate both the finite-size effect and the effect due to the free surface of a clusters.

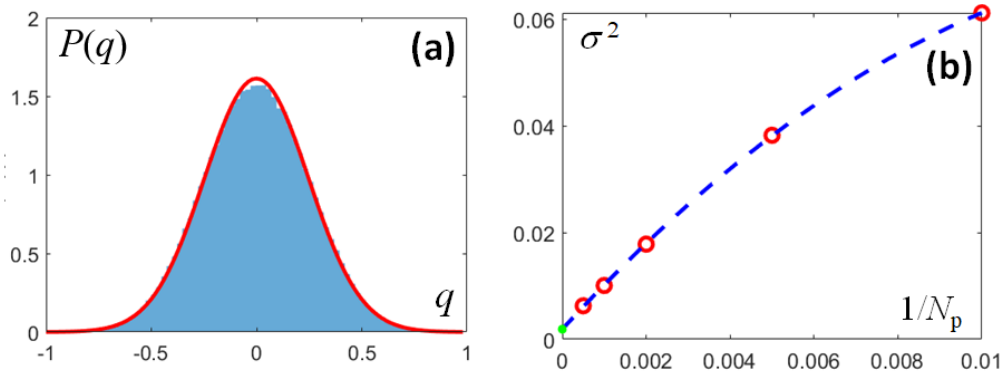

Figure 2. (**a**) Distribution density $P(q)$ of the minima overlaps (blue histogram) in a cluster of magnetic nanoparticles with reduced anisotropy $\beta = 0.5$ and the corresponding Gaussian fit (red line); (**b**) Dependence of the variance σ^2 of $P(q)$ on the inverse particle number $1/N_p$ in the cluster (red open circles) with extrapolated value for $N_p \to \infty$ (green point).

As for the desired thermodynamic limit, it can be clearly seen that the linear extrapolation of the dependence $\sigma^2(1/N_p)$ towards $1/N_p \to 0$ (i.e., in the limit $N_p \to \infty$) results in a value very close to zero. It does not extrapolate exactly to zero due to the above-mentioned presence of a free surface in our clusters: magnetic moments of particles near this surface tend to align parallel to it due to the demagnetizing field, so that small correlations of different energy minima arise. This effect becomes negligible with increasing the cluster size.

The observed behavior means that for our system in the limit $N_p \to \infty$, the distribution density of overlaps $P(q) \to \delta(q)$, so that the minima landscape behaves analogously to the landscape of a system of non-interacting particles. For this reason, we come to the conclusion that densely packed clusters of fine particles do *not* behave as a dipolar spin glass even for particles with a small single-particle anisotropy.

Unfortunately, the distribution density of overlaps is not accessible experimentally. For this reason, our results cannot be directly connected to the experimental measurements reported in papers cited above [31,32,35,40–42], where dynamical behavior similar to that

of classical atomic spin glasses was found. The detailed analysis of all these results is also out of scope of this paper. We would like only to remind the reader once more that several theoretical studies [33,41,44] have shown that both the 'memory effect' and 'aging' can be present simply in *non-interacting* systems of magnetic particles with a considerable size distribution, which leads to an exponentially broad distribution of relaxation times. The presence of interparticle interaction makes the picture qualitatively even more complicated. For all these reasons, a very careful analysis of experimental data is required to decide which of the three scenarios for the nature of the phase transition of a disordered many-particle system at low temperatures described, e.g., in subsection 2.5 of the review [39] takes place in real systems.

As for the direct comparison of our results for $P(q)$ with other numerical simulations, we are aware only of the already-mentioned comprehensive study [43], where the authors consider a system of isotropic Heisenberg dipoles (as opposed to Ising dipoles, studied in [34]) with the magnetodipolar interaction between them. In this paper, the non-zero value of the second moment σ^2 of the distribution density $P(q)$ is found for the volume fraction of particles $c \lesssim 0.49$ and below a certain transition temperature. Hence, the authors conclude that under these conditions the spin-glass phase does exist in their simulated system.

There are three main differences between our study and that performed in [43]: (i) our particles have a non-zero anisotropy, (ii) we study spherical clusters with open boundary conditions (OBCs), whereas in [43] a cubic simulation cell with periodic BCs is use, and (iii) we obtain our minima by the energy minimization from a random initial state, which corresponds to $T = 0$, whereas in [43] a Monte Carlo method is used to update system configurations, which are then used to evaluate the overlaps between them.

Considering these differences, we first note that our anisotropy is small ($\beta = 0.5$) compared to the magnetodipolar field and thus cannot have a noticeable impact on the overlap distribution $P(q)$. Secondly, open boundary conditions lead to a strong demagnetizing field and thus suppress the ferromagnetic (aligned) configuration of magnetic moments. Indeed, we did not find such a configuration for any obtained minimum, in contrast to [43], where the FM state was found for sufficiently high particle concentrations. However, a spin-glass state is highly disordered from the 'macroscopic' point of view, so the demagnetizing field due to an open surface should be nearly absent.

The most serious difference is the usage of the MC method in [43], as opposed to our zero-temperature energy minimization. This means that our local energy minima (found at $T = 0$) are definitely obtained from uncorrelated initial states. Although the authors of [43] use a strongly improved MC methodology, which allows them to 'grasp' a much larger part of the system phase space than a simple Metropolis algorithm, some correlations between subsequent states used to evaluate the interstate overlaps cannot be completely excluded. This problem is especially pronounced at low temperatures, where the spin-glass state was found in [43]. In any case, further detailed studies are necessary to clarify this issue.

3. Evaluation of Energy Barriers in Multicore Nanoclusters

3.1. Method for Calculating Energy Barriers

Now, we turn our attention to the task of determining the energy barriers between the computed energy minima of multicore clusters. Several established methods are available for calculating such barriers, including (i) the minimization of the thermodynamic action [45] (the so-called Onsager–Machlup functional (OMF) [46]), (ii) the string method [47], and (iii) the Nudged Elastic Band (NEB) method [48]. A comprehensive overview of these methods and their comparison in terms of efficiency and reliability can be found in our review [18].

Here, we have chosen to use the NEB method because, based on our experience with other physical systems, it turned out to be relatively straightforward to implement and comparatively fast. The string method is very closely related to the NEB method, but the NEB method is physically somewhat more transparent and easier to employ. Minimization of the OMF is significantly more complicated and requires a special effort to maintain the

stability of the OMF, because it contains the second derivatives of the system coordinates. In addition, the OMF has another drawback, which will be discussed in the next subsection.

Similar to other methods for finding the energy barriers, the NEB method uses the representation of a continuous path between two given local minima M_1 and M_2 as a chain of N discrete states S_i ($i = 1, \ldots, N$): $\{S_1 = M_1, S_2, \ldots, S_{N-1}, S_N = M_2\}$ (see Figure 3). In the NEB method, these states are moved according to the equation

$$\frac{\partial \mathbf{S}_i}{\partial t} = -[\nabla V(\mathbf{S}_i)]^{\perp} + \mathbf{F}_i^{\mathrm{s}} \tag{9}$$

Here, t denotes an artificially introduced time and $[\nabla V(\mathbf{S}_i)]^{\perp}$ is the component of the energy gradient perpendicular to the current transition trajectory between the minima. Moving the states along the perpendicular component of the energy gradient ensures two important properties of the (artificial) dynamics described by Equation (9): (i) all system states are moved in the direction of the decreasing energy and (ii) they are not moved along the trajectory because this movement would not contribute to the main goal of finding the saddle point.

The second term on the right-hand side in Equation (9)

$$\mathbf{F}_i^{\mathrm{s}} = k(\mathbf{S}_{i+1} - \mathbf{S}_i + \mathbf{S}_{i-1}) \tag{10}$$

is the 'spring force' that holds the states together, not allowing them to 'run away' during the minimization.

The displacement of states according to Equation (9) continues until the criterion $\|[\nabla V(\mathbf{S}_i)]^{\perp}\| < \epsilon$ ($\epsilon \ll 1$) is met, which means that all states belong to the trajectory along the energy gradient. Taking into account that the states have been always moved along the directions of decreasing energy, the obtained trajectory not only runs along the energy gradient, but also passes through the point with the minimum energy between M_1 and M_2, i.e., through the desired saddle point.

It is very important to correctly determine the tangent vector τ to the path $\{\mathbf{S}_i\}$ at each step, because this vector is required both for the calculation of the spring force and the determination of the direction perpendicular to the trajectory at the corresponding point $\mathbf{S}_i$. There are two possible first-order methods for this task. In the first method, the tangent vector is calculated as the bisector between two vectors connecting the neighbouring states (red vector in Figure 3). In the second method, it is calculated as the diagonal of the corresponding parallelogram (green vector in the same figure). In our simulations, we use the second method $\tau_i = \mathbf{S}_{i+1} - \mathbf{S}_{i-1}$, because it has proven to be more stable.

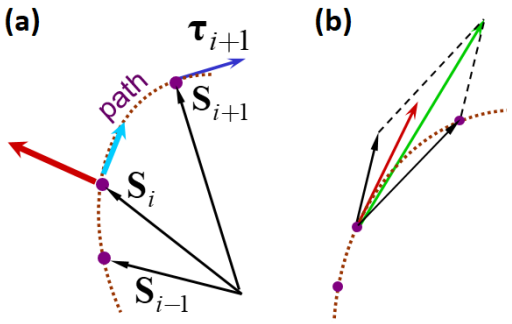

Figure 3. (**a**) The discretized path with states $\mathbf{S}_i$ and (**b**) various methods for determining the tangent τ_i to the path at state $\mathbf{S}_i$.

The only adjustable parameter in the NEB method is the spring constant k used to compute the elastic force Equation (10). When choosing k, we have to take into account the following features of NEB:

1. For too small values of k (elastic term negligible), the states are weakly connected, allowing all states to 'slide' along the trajectory into the start and end energy minima.
2. For too large values of k (elastic term dominates the motion of the states in phase space), the energy barrier height is overestimated, because the excessive spring force shortens the trajectory, causing it to pass through the point at a higher energy than the saddle point.

Therefore, making a correct choice for the spring constant k is very important. Fortunately, satisfactory results can be usually obtained in a relatively broad region of k values. Our test simulations for magnetic nanoclusters studied here have shown that the region $2 < k < 10$ provides the most accurate results.

3.2. Distinguishing Between True and False Optimal Transitions

Due to its physical transparency, the NEB method has been implemented for a large variety of physical systems, including micromagnetic ones, where it was first employed in [49,50].

The main problem with applying this method—and any other numerical method for finding the energy barrier between two metastable states—is not to find the saddle point by itself, but to ensure that the computed saddle point corresponds to the real physical transition path between the two states in question.

To understand why not every barrier found by the search for the saddle point corresponds to a physically plausible transition, let us consider a simple example: a system of two non-interacting magnetic particles, where each particle has two equivalent energy minima with magnetizations $m_z = \pm 1$ and the barrier ΔE_{1p} between them (see Figure 4). The system has four energy minima with the same energy (orientations of moments for both particles correspond to their minimal energy), marked in this figure as (1) to (4).

If we look for a transition between states (1) and (3) using NEB (or any other numerical method), we will most probably find a direct transition $(1) \longleftrightarrow (3)$ between these two states. This transition—marked in Figure 4 by the red arrow—has the barrier height $2\Delta E_{1p}$. However, the physically most probable transition goes through an intermediate state ($(1) \longleftrightarrow (2) \longleftrightarrow (3)$ or $(1) \longleftrightarrow (4) \longleftrightarrow (3)$), because for these paths the system needs to overcome two energy barriers with a height of only ΔE_{1p} each (and the probability of a transition decreases exponentially with the barrier height). Hence, the saddle point found for the direct transition $(1) \longleftrightarrow (3)$ is physically irrelevant. Below, we shall categorize such paths as 'false' optimal transitions, and transitions of the type to $(1) \longleftrightarrow (2) \longleftrightarrow (3)$ (i.e., going through the lowest saddle points) as 'true'.

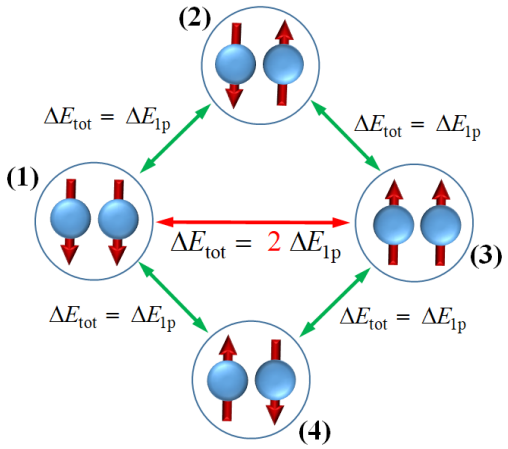

Figure 4. Explanation of the difference between 'true' and 'false' optimal transitions using the simplest non-trivial system consisting of 2 non-interacting particles each having two energy minima separated by the barrier ΔE_{1p}. See text for details.

The problem of identifying true transitions usually does not arise in standard micromagnetic systems like magnetic memory elements or multilayer stacks using spin-torque diodes, because such systems possess only two energy minima with a single saddle point or two equivalent ones between these minima. However, in interacting fine particle systems where an exponentially large number of minima with a corresponding number of saddle points in between exists (see Section 2.3), the task of distinguishing between true and false optimal transitions becomes really challenging.

We note that for the saddle point search based on OMF minimization, the problem is even more complicated. The reason is that the path between two minima found by minimizing the OMF may pass not only through a saddle point, but even through a local energy maximum (depending on the initial path guess). This unfavourable constellation is possible because the path that minimizes the OMF should proceed along the gradient lines of the energy landscape, which does not necessarily mean that it should pass via the saddle point. Indeed, it is easy to show that a trajectory along the gradient lines might also go through an energy maximum [45], providing an absolutely wrong value of the energy barrier.

To solve the problem of excluding 'false' optimal transitions (which lead to excessively high barriers) from the pool of computed optimal trajectories, we have developed the following algorithm, which was applied to each pair of energy minima:

(1) Using the NEB method, a transition path between the i-th and j-th minima was found; this transition is shown in Figure 5, where intermediate states S_i ($i = 1, \ldots, N$) are marked as blue circles.
(2) Small random perturbations in the magnetic moments of all particles in the states close to the saddle point were introduced, so that we obtained slightly different states, which are still close to the saddle.
(3) Several minimization attempts were performed starting from these states. If these attempts always ended up in one of the two minima #i or #j, then we assumed that there were no additional intermediate local minima between the states #i or #j along the transition path. Hence, this path was marked as 'true' and used to compute the corresponding energy barrier. If any different minimum was found by this procedure, then the transition was most likely not a direct transition and it was excluded from further analysis.

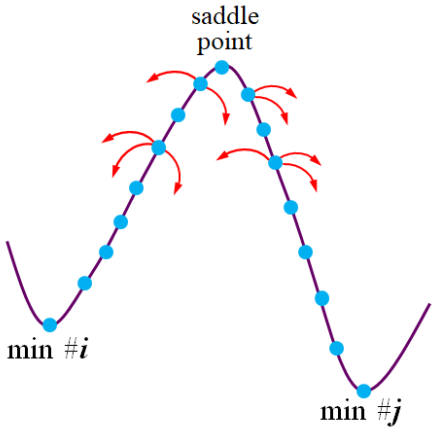

Figure 5. The principle of our method to distinguish between 'true' and 'false' optimal transitions; for this purpose, we perform small random perturbations (shown symbolically by red arrows) in the states along the optimal path, which are close to the saddle point. If energy minimization from these perturbed states leads to new minima, the path is considered as 'false'. See text for details.

3.3. Optimization of the Energy Barrier Search

The algorithm (1)–(3) described in the previous section allows us to clarify whether the already found transition between the two minima is a 'true' one and should be included

in the statistics of physically relevant energy barriers. However, the computational cost of searching for transitions between all pairs of computed minima is by itself too expensive due to the quadratic scaling $N_{\mathrm{tr}} \sim N_{\mathrm{min}}^2$ of the transition number with the number of minima.

To reduce this effort, we have employed the following idea: the probability that a transition between two minima is a 'true' one rapidly decreases when the distance between these minima increases. Therefore, it makes sense to consider only pairs of minima that are sufficiently close to each other in the sense of some metric.

The suitable metric (distance between the minima i and j) is defined as

$$\Delta m_{\mathrm{tot}}^{(i,j)} = \sum_{k}^{N_{\mathrm{p}}} \left[(\mathbf{m}_k^{(i)} - \mathbf{m}_k^{(j)})^2 \right]^{1/2} \tag{11}$$

This metric is related to the overlap defined by (7), but is constructed so that $\Delta m_{\mathrm{tot}}^{(i,j)} = 0$ if the two minima coincide (according to the definition of a metric) and is equal to $2N_{\mathrm{p}}$ if magnetic moments of minima i and j have opposite orientations for all particles.

Using this metric, we optimize the search for 'true' energy barriers in the following way.

Part A. For each minimum $\{\mathbf{m}^{(i)}\}$ from the computed minima set, we perform the following steps:

(A.1) The distances (11) between $\{\mathbf{m}^{(i)}\}$ and all other minima from this set are calculated.

(A.2) All other minima are ordered into a list according to their proximity to $\{m^{(i)}\}$. The minimum with the number l in this list is assigned to the l-th shell of neighbours.

Part B. Using the shell lists obtained in part A, the following steps are executed:

(B.1) Transition paths between all minima $\{\mathbf{m}^{(i)}\}$ and their nearest neighbours (shell #1) are calculated. For each transition, we check whether it is a 'true' one.

(B.2) Step B.1 is repeated for the next shell, until no true transitions for the current shell are found.

Our numerical experiments confirm that this approach greatly reduces the computational time, because usually no true transitions are found for the fifth nearest neighbour.

4. Distribution of Energy Barriers in Clusters of Magnetic Nanoparticles

The algorithm described above was applied to calculate energy barriers in densely packed clusters composed of nanoparticles with the diameter $D_{\mathrm{p}} = 10\,\mathrm{nm}$ and with different reduced anisotropy constants (uniaxial anisotropy type was assumed): low ($\beta = 0.5$), intermediate ($\beta = 5$), and high ($\beta = 50$) anisotropies. To obtain these values of reduced anisotropy, we assigned to the particles the magnetization value $M_{\mathrm{s}} = 400\,\mathrm{G}$ and anisotropy constants $K = 4 \times 10^4$, $K = 4 \times 10^5$, and $K = 4 \times 10^6\,\mathrm{erg/cm^3}$.

First, we note that for all anisotropies listed above we have simulated clusters containing different numbers of particles: $N_{\mathrm{p}} = 20$, 50, 80, 100. Starting from $N_{\mathrm{p}} = 50$, results are qualitatively the same (with a significantly larger number of local minima found for larger N_{p}). For this reason, we present below only results for clusters with the largest particle number $N_{\mathrm{p}} = 100$.

High single-particle anisotropy. We first simulated clusters of particles with the high anisotropy $\beta = 50$, for which magnetodipolar interaction is weak compared with the anisotropy field. For this reason, particles behave as nearly independent, so that all 'true' optimal transitions should correspond to the remagnetization of one particle.

The results of these simulations are presented in Figure 6 for the cluster containing 100 particles (results for clusters with smaller numbers of particles are nearly the same and are not shown). Part (a) of this figure shows the characteristics of the found optimal transitions on the coordinate plane (Δm_{tot}, ΔE). Here, the red circles mark the 'false' barriers, and the blue ones the 'true' barriers. It can be clearly seen that all distances Δm_{tot} defined by Equation (11) between minima connected by a 'true' transition indeed correspond to the magnetization reversal of a single particle ($\delta m = \Delta m_{1p} \approx 2$), as it should

be for this high anisotropy. Reduced energy barriers are $\Delta E/KV \approx 1$ (V is the particle volume), as also expected for a single-particle flip. This result demonstrates the robustness of our proposed method for determining physically relevant transitions.

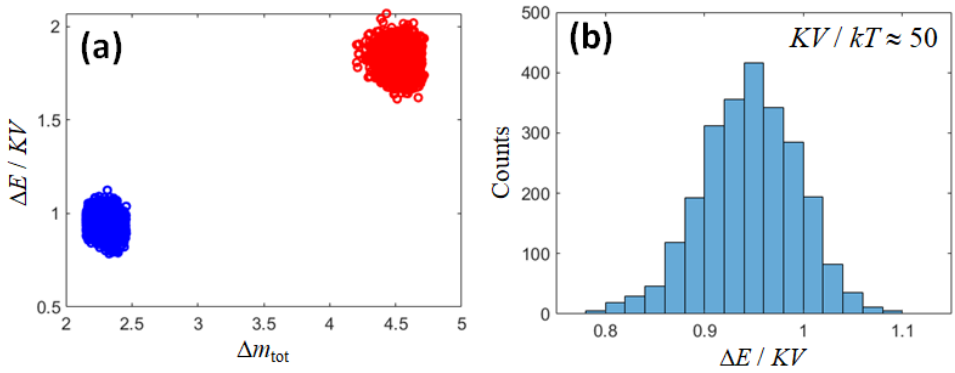

Figure 6. (**a**): Characteristics of 'true' (blue circles) and 'false' (red circles) optimal transitions shown as points on the ($\Delta E/KV$, Δm_{tot})-plane for clusters containing 100 nanoparticles with the diameter $D_{\mathrm{p}} = 10\,\mathrm{nm}$ each, and the high single-particle anisotropy $\beta = 50$. (**b**): Corresponding histogram of 'true' energy barriers. The ratio KV/kT is given for room temperature $T = 300\,\mathrm{K}$.

Figure 6b shows the histogram of 'true' energy barriers in this cluster—also in units of $\Delta E/KV$ (the histogram uses ≈ 2000 minima identified as 'true'). Interestingly, the barrier heights show a noticeable spreading around the single-particle value $\Delta E/KV = 1$, although the reduced anisotropy is very high. This means that the magnetodipolar interaction between the particles, being unable to change the individual nature of the transitions between the local minima for this system, still causes some changes in the heights of the barriers themselves. Hence, we note that the standard condition $\beta \gg 1$ for neglecting the magnetodipolar interaction in fine particle systems should be replaced in dense clusters by the stronger condition $\beta \cdot k_{\mathrm{nn}} \gg 1$, where k_{nn} is the average number of nearest neighbours; in our clusters we have $k_{\mathrm{nn}} \approx 10$.

Intermediate single-particle anisotropy. The situation for a cluster of particles with intermediate anisotropy ($K = 4.6 \times 10^5$ erg/cm^3, $M = 400$ G, so that $\beta = 5$) differs significantly from the case discussed above, as demonstrated in Figure 7. First, the existence regions of 'true' and 'false' barriers shown in Figure 7a are much broader than for $\beta = 50$, which means that already for this anisotropy the magnetodipolar interaction plays a significant role. For the same reason, the regions of existence of 'true' and 'false' barriers slightly overlap, and 'true' transitions involving moments of various numbers of particles become possible.

The distribution of 'true' energy barriers for this system displayed in the histogram in Figure 7b is also different from the case $\beta = 50$: (i) it is much broader, (ii) the maximum of this distribution is shifted towards lower barrier heights, and (iii) a significant number of very small barriers (close to zero) appear. All these effects arise because the magnetodipolar interaction no longer merely affects the barriers for individual particles, but leads to the formation of transitions involving several particles ('quasi-clusters'). For such transitions, the barrier height is determined by the interplay of the single-particle anisotropy of several particles and their magnetodipolar interaction. Due to the 'self-averaging' of the anisotropy fields in such a quasi-cluster, barriers with much lower heights can be formed.

Low single-particle anisotropy. Results for the clusters composed of 100 low-anisotropy nanoparticles with $\beta = 0.5$ are presented in Figure 8. In this case, the characteristics of energy barriers are qualitatively different both from those for $\beta = 50$ and $\beta = 5$. As can be seen from the phase diagram in panel (a), all transitions now involve many particles: the dense part of the cloud representing 'true' transitions extends up to $\Delta m_{\mathrm{tot}} \approx 40$, so that more than 20 particles can be involved. The distribution of energy barriers shown on the histogram in panel (b) (where ≈ 1000 'true' transitions are collected) is also very different

from previously discussed cases: for low anisotropy, this distribution does not have a peak at some finite barrier, but the majority of barriers are concentrated near $\Delta E = 0$. Importantly, the largest magnetization change is observed precisely for these transitions, as can be seen from the contour plot in Figure 9 (light colors correspond to a higher barrier density).

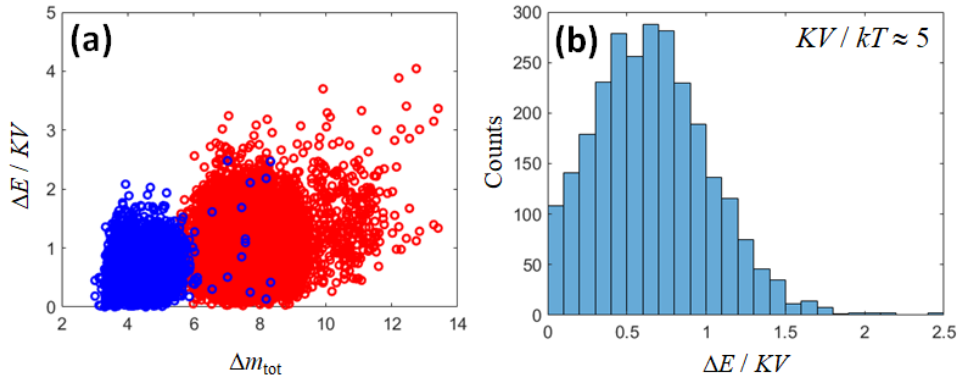

Figure 7. (**a**): Characteristics of 'true' (blue circles) and 'false' (red circles) optimal transitions shown as points on the $(\Delta E/KV,\ \Delta m_{\mathrm{tot}})$-plane for clusters containing 100 nanoparticles with the diameter $D_{\mathrm{p}} = 10\,\mathrm{nm}$ each, and the high single-particle anisotropy $\beta = 5$. (**b**): Corresponding histogram of 'true' energy barriers. The ratio KV/kT is given for room temperature $T = 300\,\mathrm{K}$.

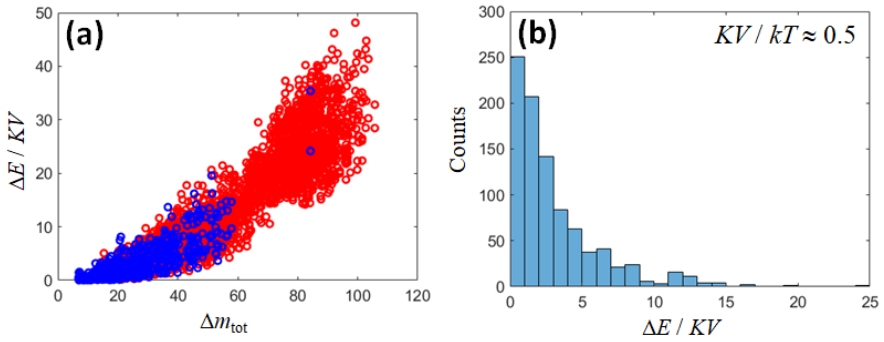

Figure 8. (**a**): Characteristics of 'true' (blue circles) and 'false' (red circles) optimal transitions shown as points on the $(\Delta E/KV,\ \Delta m_{\mathrm{tot}})$-plane for clusters containing 100 nanoparticles with the diameter $D_{\mathrm{p}} = 10\,\mathrm{nm}$ each, and the high single-particle anisotropy $\beta = 0.5$. (**b**): Corresponding histogram of 'true' energy barriers. The ratio KV/kT is given for room temperature $T = 300\,\mathrm{K}$.

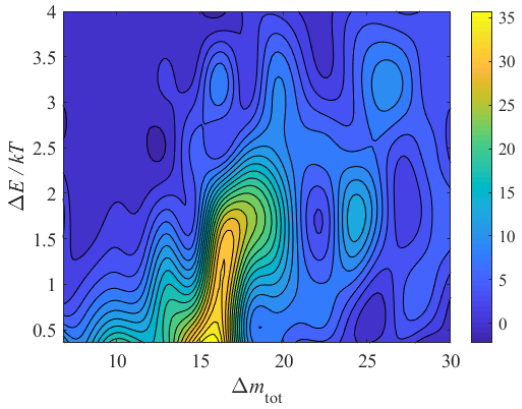

Figure 9. Contour plot for the density of energy barriers (light colors correspond to a higher density as shown on the color bar on the right) in coordinates $(\Delta m_{\mathrm{tot}}; \Delta E/kT)$ for clusters made of particles with the smallest anisotropy $\beta = 0.5$ (see also Figure 8).

Before analyzing the obtained results, we point out that the distributions of barriers in reduced units $\Delta E/KV$ shown in the figures above do not change when the particle size is changed. This follows immediately from the definition of the reduced energy Equation (3). However, the ratio of the energy barrier to the thermal energy kT obviously changes: when the particle diameter increases, e.g., by a factor of two, energy barriers in absolute units (or in kT units) increase by a factor of eight ($V \sim D_{\mathrm{p}}^3$).

Our results clearly show the role of magnetodipolar interaction in the formation of the energy barrier distribution. For very high anisotropies, this interaction leads to a moderate broadening of this distribution and its small shift toward lower barriers (we remind the reader that for non-interacting particles, this distribution is the delta-function $\rho(\Delta\widetilde{E}) \sim \delta(\Delta\widetilde{E} - 1)$, where $\widetilde{E} = \Delta E/KV$), as seen in Figure 6. For intermediate anisotropies, this broadening is much larger and a significant number of very small barriers appear (see Figure 7). For low anisotropies, the barrier distribution is entirely governed by magnetodipolar interaction: the majority of barriers are far above the non-interacting value $\Delta E/KV = 1$ and the shape of the barrier distribution changes qualitatively, with $\rho(\Delta\widetilde{E})$ monotonically decreasing with the barrier height, as demonstrated in Figure 8.

These results are qualitatively similar to those reported in our earlier study [51], where we obtained (using the minimization of the Onsager–Machlup functional) the distribution of energy barriers in a disordered system of immobile magnetic particles with volume concentrations in the region $c = 0.01 \div 0.16$ using a cubic simulation cell and periodic boundary conditions. Although this system was very different from that studied in the present paper, the qualitative trend was the same: with increasing particle concentration—which leads to the strengthening of magnetodipolar interaction—the barrier distribution shifted towards smaller barriers and for the low single-particle anisotropy $\beta = 0.2$ was qualitatively similar to the shape shown in Figure 8, already starting from $c = 0.04$. Hence, the formation of the energy barrier distribution with this characteristic shape seems to be a universal feature of magnetodipolar interaction in disordered magnetic systems.

Comparison of our findings with experimental results is difficult because measurements of the energy barrier distribution are highly non-trivial. The three most direct methods for this purpose—measurement of temperature-dependent magnetization, magnetic relaxation, and ac-susceptibility—are described in detail in the Ref. [52], where the approximations made by the interpretation of results are analyzed and the relation between these methods is discussed. Comparison of all methods in a system of Co particles with the low volume concentration of $c = 0.01$ (so that magnetodipolar interaction can be negnected) is made. The barrier distribution obtained in [52] is qualitatively similar to our results for the case of high anisotropy (Figure 6b); however, the broadening of this experimental distribution was due to the dispersion of particle sizes used in [52].

5. Discussion

Knowledge of the energy barrier distribution is not only interesting from a fundamental point of view, but is also required for the prediction of the equilibrium magnetic properties (magnetization curve and dc-susceptibility) and magnetization dynamics (mainly ac-susceptibility and magnetization relaxation) of cluster-based ferrofluids in their numerous applications.

To compute any equilibrium and dynamical properties of a system with many local minima, we have to distinguish between two regimes. If the energy barrier between the states i and j is much larger than the thermal energy ($\Delta E_{ij} \gg kT$), one can use the extended Arrhenius approximation $\Gamma_{ij}^{\mathrm{sw}} = \Gamma_{ij}^{(0)} \exp(-\Delta E/kT)$ for the prediction of the magnetization switching rate between these states. The prefactor $\Gamma_{ij}^{(0)}$ depends on several parameters of the studied system, including the energy landscape around the saddle point, so that its evaluation is a highly non-trivial task (see, e.g., [19]). In many cases, however, relatively simple expressions for this prefactor can be derived [19,53]. In addition, recently we presented the concept of the so-called 'energy-dependent temperature' [54], which allows

us to evaluate the switching rate numerically without any approximations by an advanced single-stage Langevin dynamics method.

In this high-barrier regime, the knowledge of $\Gamma_{ij}^{(0)}$ allows us to evaluate all dynamic properties of the cluster-based systems using well-known approaches. Namely, for the total ac-susceptibility the textbook result for the susceptibility $\chi_{ij}(\omega)$ corresponding to the transition $i \leftrightarrow j$ can be used, with subsequent averaging over all such pairs. For prediction of magnetic relaxation after a sudden change in the external field, the system of differential equations describing the time evolution of the population of system states should be solved; the matrix elements of this system are equal to switching rates $\Gamma_{ij}^{(0)}$.

If the condition $\Delta E \gg kT$ is not met, the approximation $\Gamma_{\mathrm{sw}} \sim \exp(-\Delta E/kT)$ becomes invalid, because the two corresponding states are not well defined: thermal fluctuations 'smear them out' and it is not possible to compute their populations separately. In this case, Langevin dynamics simulations should be employed.

As an example, for magnetic particles with the size $D_{\mathrm{p}} = 10\,\mathrm{nm}$ the ratio $\Delta E/kT$ at room temperature $T = 300\,\mathrm{K}$ is shown in panel (b) in Figures 6–8. It varies from $\Delta E/kT = 50$ for the particles with the highest anisotropy to $\Delta E/kT = 0.5$ for the smallest anisotropy case. This means that the Arrhenius law and its refinements [19] can be used in this example, strictly speaking, only for particles with $K = 4 \times 10^6\,\mathrm{erg/cm^3}$ ($\beta = 50$). Already for the intermediate anisotropy, the Arrhenius approximation is not valid, so that both for this anisotropy and for $K = 4 \times 10^4\,\mathrm{erg/cm^3}$ full-scale Langevin dynamics simulations are clearly necessary. This is especially true in the latter case, because at $K = 4 \times 10^4\,\mathrm{erg/cm^3}$ the majority of transitions have energy barriers close to zero, and magnetization changes for these transitions are not small, as shown in Figure 9.

When the particle diameter is increased, all histograms of energy barriers presented in Figures 6–8 remain the same, because the reduced energy Equation (3) used in all our methods is already in units of KV. However, the ratio KV/kT—displayed in panel (b) of these figures—changes, following the change in the particle volume. For example, for particles with a diameter twice as much ($D_{\mathrm{p}} = 20\,\mathrm{nm}$), this ratio increases by $8\times$, so that for the moderate anisotropy $\beta = 5$ the energy barriers will also fulfill the condition $\Delta E/kT \gg kT$ for the majority of the interstate transitions (see Figure 7b).

However, for clusters consisting of particles with a small anisotropy ($\beta = 0.5$) the Arrhenius approximation remains invalid, because the main contribution to the density of energy barriers comes from barriers close to zero ($\rho(\Delta E/KV)$ seems even to diverge at $\Delta E = 0$). For this reason, dynamical system properties must be studied using Langevin dynamics simulations.

6. Conclusions

The results of our simulations of local energy minima and the energy barriers between them in dense clusters of magnetic particles can be summarized as follows.

Analyzing the structure of the landscape of energy minima, we have not found any features expected for the spin-glass state. In particular, using our highly efficient algorithms for minimizing the system energy, we could obtain a large number of local minima (at $T = 0$), starting from arbitrary orientations of magnetic moments. This way, we computed the distribution density of overlaps between these minima with a very high statistical accuracy. This density was found to be Gaussian, and its width unambiguously tends to zero in the macroscopic limit of the particle number ($N_{\mathrm{p}} \to \infty$), analogously to the system of non-interacting particles with randomly oriented anisotropy axes.

Further, we have developed a reliable method for finding the 'true' optimal transition path between two given energy minima and to evaluate the corresponding energy barrier. This method has allowed us to compute a large number of these barriers and to determine their distribution density for clusters made of particle with various anisotropies. We have shown that these distributions are qualitatively different for systems of particles with low, intermediate, and high anisotropies. Whereas for particles with a high anisotropy, the distribution of barriers has a well-defined peak at the single-particle energy barrier, for the

case of low anisotropy the distribution is concentrated near very small barriers, and even seems to diverge at $\Delta E \to 0$. We also point out that for dense particle clusters single-particle behavior is observed only for reduced anisotropy values obeying the condition $\beta N_{\mathrm{nn}} \gg 1$ (N_{nn} being the number of nearest neighbors), which is stronger than the 'standard' condition $\beta \gg 1$.

Both groups of results summarized above have important implications for the analysis of the dynamic behavior of magnetic systems containing dense particle clusters, in particular for aggregated ferrofluids with their numerous potential applications in medicine.

Author Contributions: Conceptualization, D.B.; formal analysis, N.L.G. and E.K.S.; funding acquisition, D.B.; investigation, D.B., N.L.G., and E.K.S.; methodology, N.L.G.; project administration, D.B.; software, N.L.G. and E.K.S.; validation, D.B., N.L.G., and E.K.S.; visualization, N.L.G.; writing—original draft, D.B. All authors have read and agreed to the published version of the manuscript.

Funding: This research was funded by the German Federal Ministry for Economic Affairs and Climate Action, Inno-Kom funding program, grant number 49MF200010.

Data Availability Statement: The original contributions presented in this study are included in the article. Further inquiries can be directed to the corresponding author.

Conflicts of Interest: The authors declare no conflicts of interest.

References

1. Liu, X.; Chen, H.; Chen, X.; Alfadhl, Y.; Yu, J.; Wen, D. Radiofrequency heating of nanomaterials for cancer treatment: Progress, controversies, and future development. *Appl. Phys. Rev.* **2015**, *2*, 011103. [CrossRef]
2. Périgo, E.; Hemery, G.; Sandre, O.; Ortega, D.; Garaio, E.; Plazaola, F.; Teran, F.J. Fundamentals and advances in magnetic hyperthermia. *Appl. Phys. Rev.* **2015**, *2*, 041302. [CrossRef]
3. Angioletti-Uberti, S. Theory, simulations and the design of functionalized nanoparticles for biomedical applications: A Soft Matter Perspective. *NPJ Comp. Mat.* **2017**, *3*, 48. [CrossRef]
4. El-Boubbou, K. Magnetic iron oxide nanoparticles as drug carriers: Clinical relevance. *Nanomedicine* **2018**, *13*, 953. [CrossRef]
5. Krasia-Christoforou, T.; Socoliuc, V.; Knudsen, K.D.; Tombácz, E.; Turcu, R.; Vékás, L. From Single-Core Nanoparticles in Ferrofluids to Multi-Core Magnetic Nanocomposites. *Nanomaterials* **2020**, *10*, 2178. [CrossRef]
6. Gubin, S. *Magnetic Nanoparticles*; Wiley-VCH: Weinheim, Germany, 2009.
7. Taylor, R.; Coulombe, S.; Otanicar, T.; Phelan, P.; Gunawan, A. Small particles, big impacts: A review of the diverse applications of nanofluids. *J. Appl. Phys.* **2013**, *113*, 011301. [CrossRef]
8. Plouffe, B.; Murthy, S.; Lewis, L. Fundamentals and application of magnetic particles in cell isolation and enrichment: A review. *Rep. Prog. Phys.* **2015**, *78*, 016601. [CrossRef] [PubMed]
9. Vallabani, N.S.; Singh, S. Recent advances and future prospects of iron oxide nanoparticles in biomedicine and diagnostics. *Biotech* **2018**, *8*, 279. [CrossRef]
10. Dutz, S.; Hergt, R. Magnetic particle hyperthermia—A promising tumour therapy? *Nanotechnology* **2014**, *25*, 452001. [CrossRef] [PubMed]
11. Pourmiri, S.; Tzitzios, V.; Hadjipanayis, G.; Brassea, B.M.; El-Gendy, A. Magnetic properties and hyperthermia behavior of iron oxide nanoparticle clusters. *AIP Adv.* **2019**, *9*, 125033. [CrossRef]
12. Wu, K.; Su, D.; Saha, R.; Wong, D.; Wang, J.P. Magnetic Particle Spectroscopy-based Bioassays: Methods, Applications, Advances, and Future Opportunities. *J. Phys. D Appl. Phys.* **2019**, *52*, 173001. [CrossRef]
13. Talebloo, N.; Gudi, M.; Robertson, N.; Wang, P. Magnetic Particle Imaging: Current Applications in Biomedical Research. *J. Magn. Res. Imaging* **2020**, *51*, 1659. [CrossRef] [PubMed]
14. Ivanov, A.; Camp, P. Theory of the dynamic magnetic susceptibility of ferrofluids. *Phys. Rev. E* **2018**, *98*, 050602(R). [CrossRef]
15. Solovyova, A.Y.; Elfimova, E.A.; Ivanov, A.O.; Camp, P.J. Modified mean-field theory of the magnetic properties of concentrated, high-susceptibility, polydisperse ferrofluids. *Phys. Rev. E* **2017**, *96*, 052609. [CrossRef]
16. Lebedev, A.V.; Stepanov, V.I.; Kuznetsov, A.A.; Ivanov, A.O.; Pshenichnikov, A.F. Dynamic susceptibility of a concentrated ferrofluid: The role of interparticle interactions. *Phys. Rev. E* **2019**, *100*, 032605. [CrossRef] [PubMed]
17. Berkov, D.; Gorn, N.; Schmitz, R.; Stock, D. Langevin dynamic simulations of fast remagnetization processes in ferrofluids with internal magnetic degrees of freedom. *J. Phys. Cond. Matt.* **2006**, *18*, S2595. [CrossRef]
18. Berkov, D. Magnetization dynamics including thermal fluctuations: Basic phenomenology, fast remagnetization processes and transitions over high-energy barriers. In *Handbook of Magnetism and Advanced Magnetic Materials*; Kronmüller, H., Parkin, S., Eds.; John Wiley & Sons, Ltd.: Chichester, UK, 2007; Volume 2: Micromagnetism, pp. 795–823.
19. Coffey, W.; Kalmykov, Y. Thermal fluctuations of magnetic nanoparticles: Fifty years after Brown. *J. Appl. Phys.* **2012**, *112*, 121301. [CrossRef]

20. Lyutyy, T.; Hryshko, O.; Kovner, A. Power loss for a periodically driven ferromagnetic nanoparticle in a viscous fluid: The finite anisotropy aspects. *J. Magn. Magn. Mater.* **2018**, *446*, 87–94. [CrossRef]
21. Zubarev, A.Y. Magnetic hyperthermia in a system of ferromagnetic particles, frozen in a carrier medium: Effect of interparticle interactions. *Phys. Rev. E* **2018**, *98*, 032610. [CrossRef]
22. Dutz, S.; Kettering, M.; Hilger, I.; Müller, R.; Zeisberger, M. Magnetic multicore nanoparticles for hyperthermia—influence of particle immobilization in tumour tissue on magnetic properties. *Nanotechnology* **2011**, *22*, 265102. [CrossRef]
23. Nishimoto, K.; Ota, S.; Shi, G.; Takeda, R.; Trisnanto, S.; Yamada, T.; Takemura, Y. High intrinsic loss power of multicore magnetic nanoparticles with blood-pooling property for hyperthermia. *AIP Adv.* **2019**, *9*, 035347. [CrossRef]
24. Kahmann, T.; Ludwig, F. Magnetic field dependence of the effective magnetic moment of multi-core nanoparticles. *J. Appl. Phys.* **2020**, *127*, 233901. [CrossRef]
25. Kuznetsov, A. Force acting on a cluster of magnetic nanoparticles in a gradient field: A Langevin dynamics study. *J. Magn. Magn. Mat.* **2019**, *475*, 415–420. [CrossRef]
26. Trisnanto, S.; Takemura, Y. Dipolar field-induced asymmetric magnetization hysteresis of immobile superparamagnetic nanoclusters. *J. Magn. Magn. Mat.* **2019**, *480*, 132–137. [CrossRef]
27. Ivanov, A.; Ludwig, F. Static magnetic response of multicore particles. *Phys. Rev. E* **2020**, *102*, 032603. [CrossRef] [PubMed]
28. Usov, N.A.; Serebryakova, O.N.; Tarasov, V.P. Interaction Effects in Assembly of Magnetic Nanoparticles. *Nanoscale Res. Lett.* **2017**, *12*, 489. [CrossRef] [PubMed]
29. Abu-Bakr, A.; Zubarev, A. Effect of ferromagnetic nanoparticles aggregation on magnetic hyperthermia. *Eur. Phys. J. Spec. Top.* **2020**, *229*, 323–329. [CrossRef]
30. Ilg, P. Equilibrium magnetization and magnetization relaxation of multicore magnetic nanoparticles. *Phys. Rev. B* **2017**, *95*, 214427. [CrossRef]
31. Parker, D.; Dupuis, V.; Ladieu, F.; Bouchaud, J.P.; Dubois, E.; Perzynski, R.; Vincent, E. Spin-glass behavior in an interacting γ-Fe_2O_3 nanoparticle system. *Phys. Rev. B* **2008**, *77*, 104428. [CrossRef]
32. Cador, O.; Grasset, F.; Haneda, H.; Etourneau, J. Memory effect and super-spin-glass ordering in an aggregated nanoparticle sample. *J. Magn. Magn. Mater.* **2004**, *268*, 232–236. [CrossRef]
33. Bandyopadhyay, M.; Dattagupta, S. Memory in nanomagnetic systems: Superparamagnetism versus spin-glass behavior. *Phys. Rev. B* **2006**, *74*, 214410. [CrossRef]
34. Fernandez, J.F. Monte Carlo study of the equilibrium spin-glass transition of magnetic dipoles with random anisotropy axes. *Phys. Rev. B* **2008**, *78*, 064404. [CrossRef]
35. Konwar, K.; Kaushik, S.D.; Sen, D.; Deb, P. Dynamic spin freezing and magnetic memory effect in ensembles of interacting anisotropic magnetic nanoparticles. *Phys. Rev. B* **2020**, *102*, 174449. [CrossRef]
36. Jodrey, W.S.; Tory, E.M. Computer simulation of close random packing of equal spheres. *Phys. Rev. A* **1985**, *32*, 2347–2351. [CrossRef]
37. Berkov, D. Numerical simulations of quasistatic remagnetization processes in fine magnetic particle systems. *J. Magn. Magn. Matt.* **1996**, *161*, 337–356. [CrossRef]
38. Binder, K.; Young, A. Spin Glasses: Experimental facts, theoretical concepts and open questions. *Rev. Mod. Phys.* **1986**, *58*, 801.
39. Dotsenko, V. Physics of the spin-glass state. *Phys.-Uspekhi* **1993**, *36*, 455. [CrossRef]
40. Chen, X.; Bedanta, S.; Petracic, O.; Kleemann, W.; Sahoo, S.; Cardoso, S.; Freitas, P.P. Superparamagnetism versus superspin glass behavior in dilute magnetic nanoparticle systems. *Phys. Rev. B* **2005**, *72*, 214436. [CrossRef]
41. Sasaki, M.; Jonsson, P.E.; Takayama, H.; Mamiya, H. Aging and memory effects in superparamagnets and superspin glasses. *Phys. Rev. B* **2005**, *71*, 104405. [CrossRef]
42. Suzuki, M.; Fullem, S.I.; Suzuki, I.S.; Wang, L.; Zhong, C.J. Observation of superspin-glass behavior in Fe3O4 nanoparticles. *Phys. Rev. B* **2009**, *79*, 024418. [CrossRef]
43. Alonso, J.J.; Alles, B.; Russier, V. Magnetic ordering of random dense packings of freely rotating dipoles. *Phys. Rev. B* **2020**, *102*, 184423. [CrossRef]
44. Viddal, C.A.; Roshko, R.M. Aging and memory effects in zero-field-cooled collections of two-level subsystems. *Phys. Rev. B* **2006**, *73*, 172416. [CrossRef]
45. Berkov, D. Numerical calculation of the energy barrier distribution in disordered many-particle systems: The path integral method. *J. Magn. Magn. Mat.* **1998**, *186*, 199–213. [CrossRef]
46. Onsager, L.; Machlup, S. Fluctuations and irreversible processes. *Phys. Rev.* **1953**, *91*, 1505. [CrossRef]
47. E, W.; Ren, W.; Vanden-Eijnden, E. String method for the study of rare events. *Phys. Rev. B* **2002**, *60*, 052301. [CrossRef]
48. Jonsson, H.; Mills, G.; Jacobsen, K., Nudged elastic band method for finding minimum energy paths of transitions. In *Classical and Quantum Dynamics in Condensed Phase Simulations*; World Scientific: Singapore, 1998; Chapter 16, pp. 385–404. [CrossRef]
49. Dittrich, R.; Schrefl, T.; Suess, D. A path method for finding energy barriers and minimum energy paths in complex micromagnetic systems. *J. Magn. Magn. Mat.* **2002**, *250*, 12–19. [CrossRef]
50. Dittrich, R.; Schrefl, T.; Forster, H. Energy barriers in magnetic random access memory elements. *IEEE Trans. Magn.* **2003**, *39*, 2839–2841. [CrossRef]
51. Berkov, D. Density of energy barriers in fine magnetic particle systems. *IEEE Trans. Magn.* **2002**, *38*, 2637–2639. [CrossRef]

52. Zheng, R.; Gu, H.; Zhang, B.; Liu, H.; Zhang, X.; Ringer, S.P. Extracting anisotropy energy barrier distributions of nanomagnetic systems from magnetization/susceptibility measurements. *J. Magn. Magn. Mater.* **2009**, *321*, L21–L27. [CrossRef]
53. Semenova, E.K.; Berkov, D.V.; Gorn, N.L. Evaluation of the switching rate for magnetic nanoparticles: Analysis, optimization, and comparison of various numerical simulation algorithms. *Phys. Rev. B* **2020**, *102*, 144419. [CrossRef]
54. Berkov, D.; Semenova, E.K.; Gorn, N.L. Single-stage direct Langevin dynamic simulations of transitions over arbitrarily high energy barriers: Concept of energy-dependent temperature. *Phys. Rev. B* **2021**, *104*, 224408. [CrossRef]